

## Seismic Attenuation in Northeastern Sonora, Mexico

by Raúl R. Castro, Cristina Condori, Oscar Romero, César Jacques, and Max Suter

**Abstract** We studied the attenuation of local and regional earthquake body waves recorded by the seismic network of northeastern Sonora, Mexico (Red Sísmica del Noreste de Sonora [RESNES]). The source-station paths of the selected data set cover the epicentral region of the May 1887 ( $M_w$  7.5) Sonora earthquake. We used the best-located earthquakes recorded by RESNES between 2003 and 2004 to analyze the spectral amplitude decay of body waves with hypocentral distance. The database consists of 44 earthquakes with magnitudes between 1.8 and 3.2 and hypocentral distances between 25 and 150 km. We calculated Fourier spectral amplitudes from more than 400 records and defined attenuation functions with a nonparametric model by inverting the observed spectral amplitudes at 23 individual frequencies between 0.4 and 63.1 Hz. We determined regional attenuation curves based on events located more than 100 km northwest of the center of the network and local curves based on earthquakes located near the fault zone that ruptured in the 1887 earthquake. The obtained attenuation curves indicate that the spectral amplitudes decay faster in the area of the 1887 rupture than in the surrounding region. To analyze the possible sources of attenuation, we parameterized the attenuation functions considering three terms: one that accounts for geometrical spreading, another one for anelastic attenuation, and a third for near-surface attenuation. We found the  $S$ -wave quality factor  $Q$  to be similar in both the general region and near the 1887 rupture. However, in the region of the 1887 rupture, the near-surface attenuation exceeds the regional average. Finally, in the region of the 1887 rupture, the nonparametric attenuation functions and the estimates of  $Q$  indicate that at between 0.6 and 63.1 Hz,  $P$  waves attenuate more than  $S$  waves ( $Q_P = 20.8f^{1.1}$ , whereas  $Q_S = 83.8f^{0.9}$ ).

### Introduction

In northeastern Sonora, north–south striking, west-dipping normal faults form the limit between the Sonoran Basin and Range (Brand, 1937) a subprovince of the southern Basin and Range province in the west and the less extended plateau of the Sierra Madre Occidental in the east (Fig. 1). These faults and associated half-grabens extend over a distance of more than 300 km between the San Bernardino basin in the north and the Sahuaripa basin in the south. A large earthquake in 1887, with a surface rupture length of 101.8 km and  $M_w$  7.5 (Bakun, 2006; Suter, 2006), ruptured three neighboring segments of this major fault zone; from south to north these segments are mapped as the Otates, Teras, and Pitáycachi faults (Fig. 1; Suter and Contreras, 2002).

On a larger scale, the faults of the Sonoran Basin and Range province are part of the extension that surrounds the less deformed plateau of the Sierra Madre Occidental (Stewart, 1998; Henry and Aranda-Gómez, 2000). This extension is ongoing; the number of faults in the Mexican part of the southern Basin and Range known to have been active

during the Quaternary is increasing with each new investigation (e.g., Aranda-Gómez *et al.*, 2003; Suter, 2004; Aguirre-Díaz *et al.*, 2005), and historical seismicity is abundant (e.g., Doser and Rodríguez, 1993; Yamamoto, 1993; García Acosta and Suárez Reynoso, 1996; Suter *et al.*, 1996; Suter, 2001; Suter and Contreras, 2002; Zúñiga *et al.*, 2003). Furthermore, borehole elongations in the Mexican part of the southern Basin and Range province show that the least horizontal stress is oriented approximately east–west, perpendicular to the traces of major normal faults (Suter, 1991).

Recently, the seismic network Red Sísmica del Noreste de Sonora (RESNES) was installed in this region to document seismicity likely related with the Basin and Range faults of northeastern Sonora (Castro *et al.*, 2002; Romero *et al.*, 2004). The network consists of nine digital stations that record three components of acceleration and the vertical component of ground velocity. Figure 1 (triangles) shows the locations of the stations that operated during the period 2003–2004; 13 stations are shown because some of them were relocated, but only nine stations have been operating

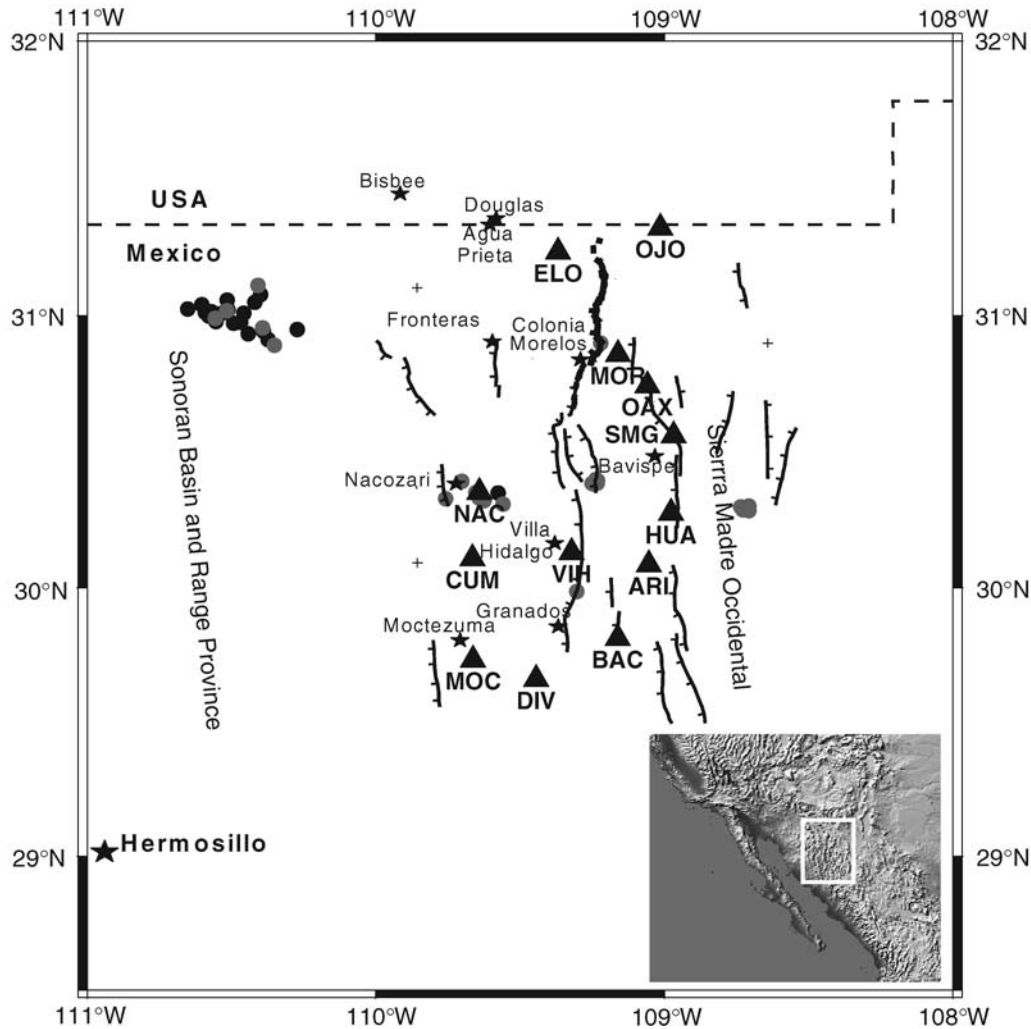


**Figure 1.** Location of the study area. Lines indicate major Basin and Range faults (the thick line is the 1887 surface rupture along the western margin of the Sierra Madre occidental). The location of the stations, triangles; major population centers, stars; the epicentral locations, circles. Fault traces and 1887 surface rupture trace were taken from Suter and Contreras (2002).

simultaneously. Additionally, station NE81 (Fig. 1), a broadband station belonging to the network of autonomously recording seismographs (NARS) Baja array (Trampert *et al.*, 2003) was also used to locate some of the epicenters.

In this article, we analyze local and regional events recorded by the RESNES array to characterize, for the first time, the seismic attenuation of northeastern Sonora, México. We determine empirical attenuation functions that describe the spectral amplitude decay with distance at individual frequencies and then use these functions to estimate the quality factor  $Q$ .

#### Data

We selected the records of 44 earthquakes located inside the RESNES array and near Cananea, a town about 100 km northwest of the center of the array (Fig. 1). These events have hypocentral distances between 25 and 150 km and magnitudes between 1.8 and 3.2. Figure 2 displays the distribution of earthquake magnitudes versus hypocentral distance of

the selected events and indicates that most of the events have magnitudes above 2.0.

The RESNES stations consist of Kinemetrics K2 digital four-channel recorders with an internal triaxial force-balance accelerometer (EpiSensor) and a built-in Global Positioning System (GPS) timing system. Three channels record the vertical, the north-south, and the east-west components of ground acceleration, and the fourth channel is connected to a vertical-component short-period sensor (model L4C) that records ground velocity. These stations are set to record local and regional earthquakes with a rate of 200 samples per second.

The selected records were baseline corrected to remove long-period biases by subtracting the mean. We then chose time windows containing clear  $P$ - and  $S$ -wave arrivals to calculate the acceleration spectra. The first and last 5% of the selected windows were cosine tapered, and the spectral amplitudes were smoothed using a variable frequency band of  $\pm 25\%$  of 23 predefined frequencies between 0.4 and

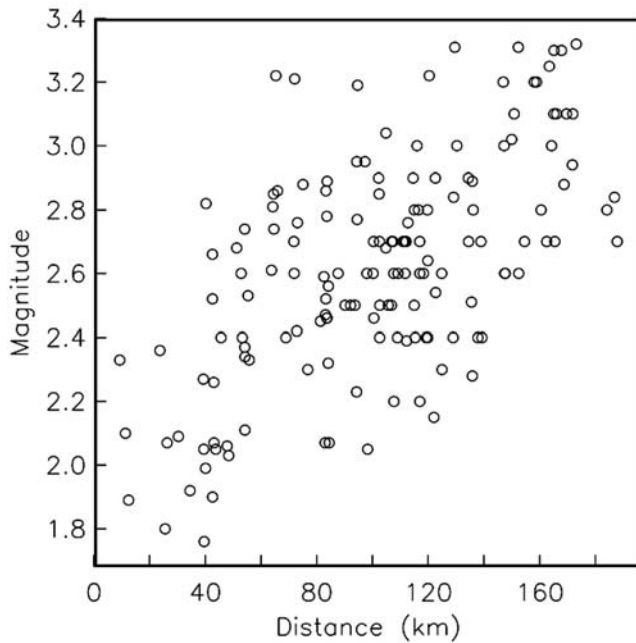


**Figure 2.** Distribution of earthquake magnitude versus hypocentral distance.

63.1 Hz. The spectral records were also visually inspected to select frequency bands containing amplitudes useful for further analysis. Figure 3 shows the *S*-wave east-component acceleration spectra of two events recorded at various hypocentral distances. For both events, the spectral amplitudes decay considerably with distance. For instance, the spectral amplitudes at 10 Hz of the *M* 2.8 event (right frame in Fig. 3) decay by a factor of 12 between the station located at 23.7 km and the one at 135.9 km.

To analyze the possible spatial variation of the attenuation, we divided the data set in two groups: one with the epi-

central locations northwest of the array, whose source-station paths have a regional coverage (Fig. 4) and a second group with source-station paths sampling the 1887 rupture zone (Fig. 5). Most of the events of the first group, recorded during 2003, have clear *S*-wave traces only in the velocity channel, whereas the second group, recorded during 2004, has useful signals in all four channels.

### Methodology

We determined empirical functions that describe the observed trends of the spectral amplitude decay with distance using a nonparametric method (e.g., Anderson and Quaa, 1988; Castro *et al.*, 1990; Anderson and Lei, 1994; Castro *et al.*, 1996). The dependence of the spectral amplitudes  $U$  on hypocentral distance  $r$  for a given frequency  $f$  was modeled as

$$U_i(f, r) = S_i(f)A(f, r), \quad (1)$$

where  $U_i(f, r)$  is the observed spectral amplitude of event  $i$ ,  $A(f, r)$  is the empirically determined attenuation function that describes the distance decay trend, and  $S_i(f)$  is a scalar (one for each earthquake  $i$  at frequency  $f$ ) that depends on the size of the earthquake.  $A(f, r)$  contains the effects of both the geometrical spreading and the quality factor  $Q$  but is not limited to a particular functional form. Instead of constraining the attenuation functions to decay exponentially with distance or to any other functional form, we searched for unrestricted monotonic curves constrained to a reasonable degree of smoothness. With this approach, the site effects are the residuals resulting from solving equation (1). This technique was introduced by Brillinger and Preisler (1984) for the analysis of attenuation relations of peak accelerations. Richter (1935) used a similar method to develop the local

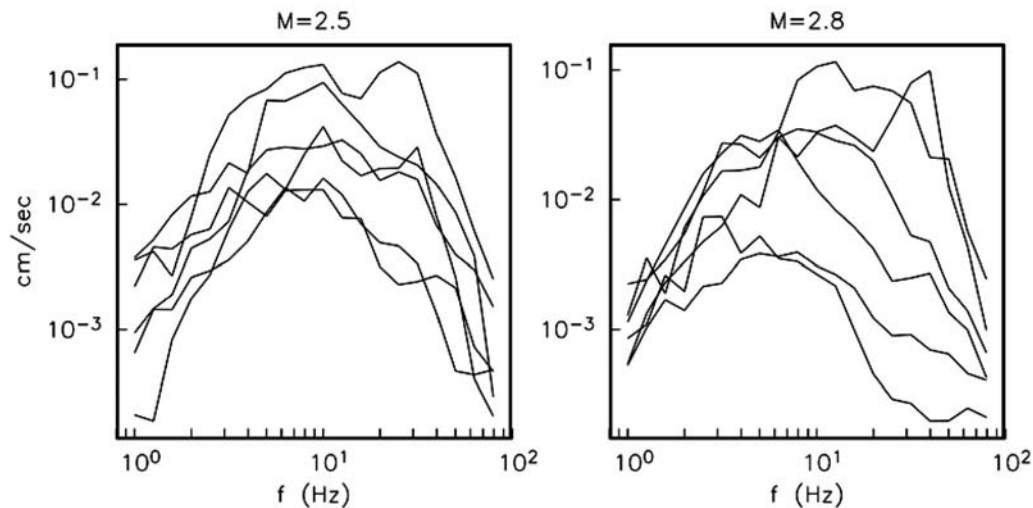


**Figure 3.** *S*-wave acceleration spectra calculated from east components of two selected earthquakes. The left frame corresponds to an *M* 2.5 earthquake recorded at 25.6–139.0-km distance and the right frame to an *M* 2.8 earthquake recorded between 23.7 and 135.9 km from its epicenter.

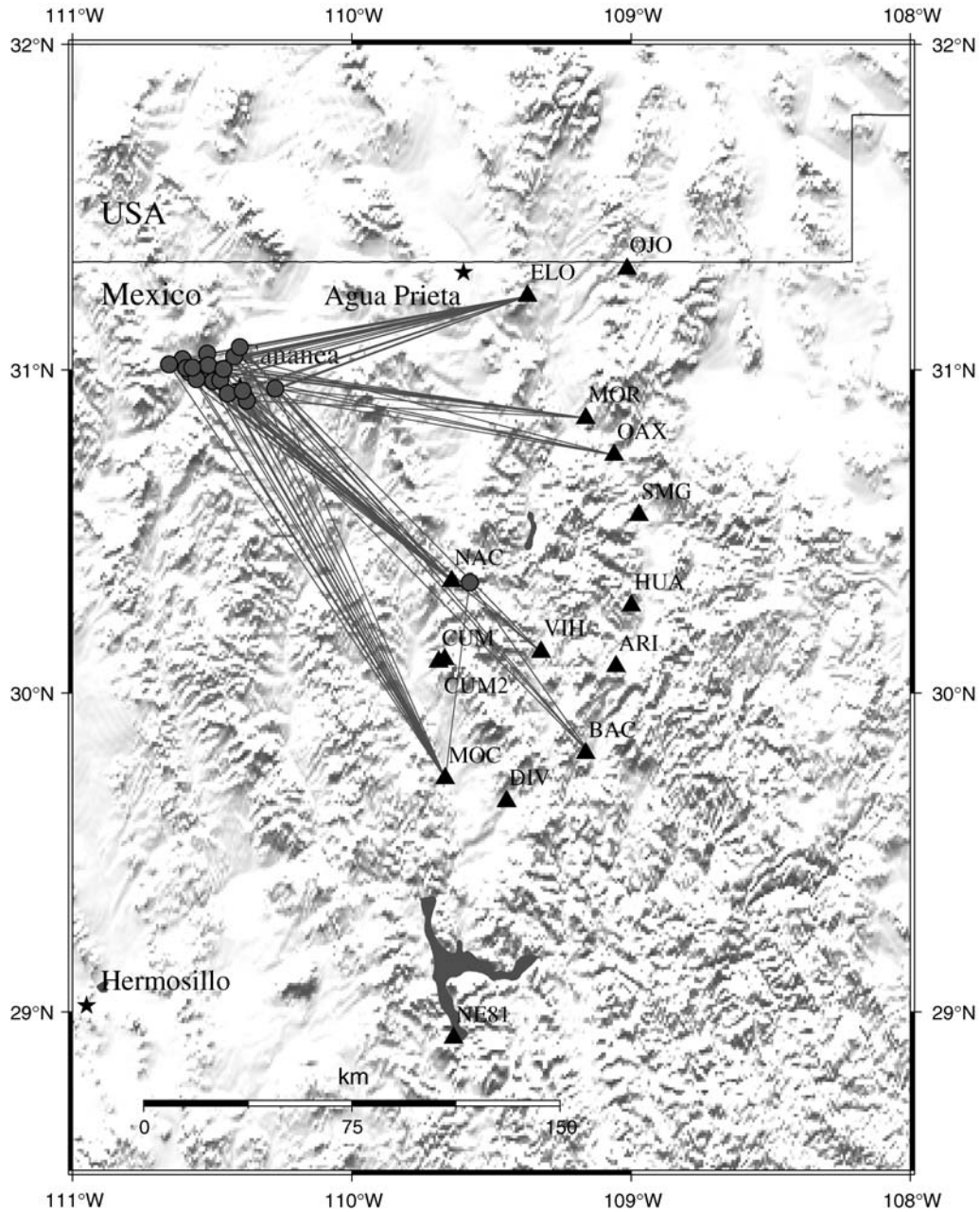


**Figure 4.** Map showing source-station paths of regional earthquakes recorded by stations located on the western side of the fault zone that delimits the plateau of the Sierra Madre occidental, and which ruptured partly in an  $M_w$  7.5 earthquake in 1887.

magnitude scale for southern California, and more recently this nonparametric approach has been used by other authors as well (Raouf *et al.*, 1999; Malagnini *et al.*, 2000; Spallarosa *et al.*, 2002; Ortega and Quintanar, 2005) to find attenuation relations.

Because at  $r = 0$  the spectral amplitudes are fully governed by the source term  $S_i(f)$ , we constrained the attenuation functions to be 1 at  $r = 0$  ( $A(f, 0) = 1.0$ ). We also assumed the shape of the attenuation function at a given frequency to be the same for all the earthquakes regardless of the magnitude, so that we can invert equation (1) using all the events simultaneously. The advantage of this method is that

the spectral amplitudes from small and larger events complement each other to define the attenuation function.

From equation (1), we formed at each frequency a set of linear equations of the form

$$u_{ij} = s_i + a_j, \tag{2}$$

where  $u_{ij} = \log U_i(f, r)$  is a datum from earthquake  $i$  at distance  $j$ ,  $s_i = \log S_i(f)$ , and  $a_j = \log A(f, r)$  is the value of the attenuation function at distance  $j$ .

Equation (2) represents a system of equations that is solved by a constrained least-squares inversion and can be

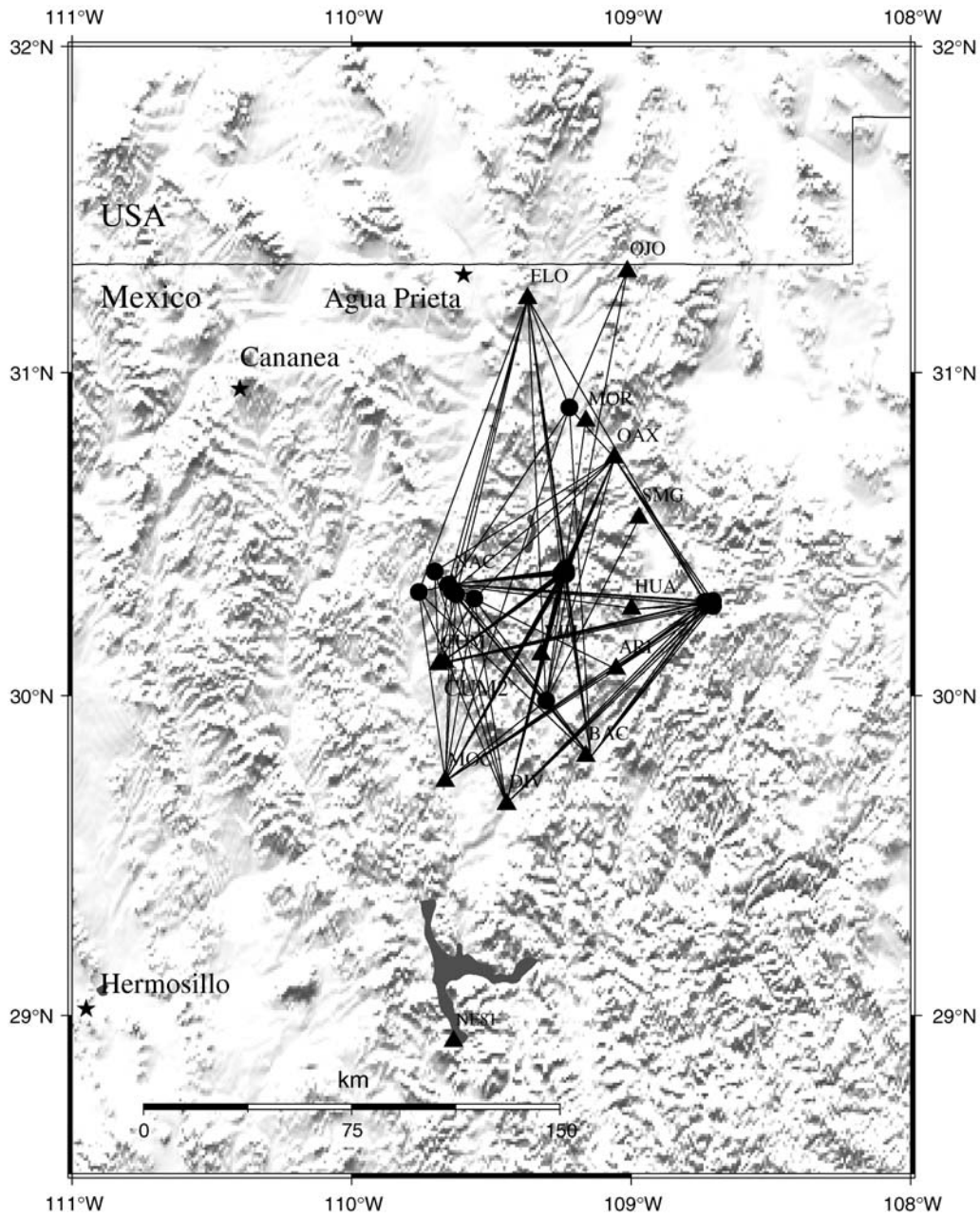


**Figure 5.** Map with source-station paths of local earthquakes recorded by RESNES array in the region of the 1887 earthquake rupture.

written in matrix form as

$$\begin{pmatrix}
 1 & 0 & 0 & \cdot & \cdot \\
 0 & 1 & 0 & \cdot & \cdot \\
 \cdot & \cdot & \cdot & \cdot & \cdot \\
 \cdot & \cdot & \cdot & \cdot & \cdot \\
 w_1 & 0 & 0 & \cdot & \cdot \\
 -w_2/2 & w_2 & -w_2/2 & 0 & \cdot \\
 0 & -w_2/2 & w_2 & \cdot & \cdot \\
 \cdot & \cdot & \cdot & \cdot & \cdot
 \end{pmatrix}
 \begin{pmatrix}
 a_1 \\
 \cdot \\
 \cdot \\
 a_j \\
 s_1 \\
 \cdot \\
 \cdot \\
 s_i
 \end{pmatrix}
 =
 \begin{pmatrix}
 u_{11} \\
 \cdot \\
 \cdot \\
 u_{ij} \\
 0 \\
 0 \\
 \cdot \\
 \cdot
 \end{pmatrix},
 \tag{3}$$

where  $w_1$  and  $w_2$  are weighting factors used to constrain  $a_1 = 0$  at  $r = 0$  and to weight the second derivative for smoothing purposes, respectively. The selected value of  $w_2$  and the resulting model parameters  $a_j$  define the shape of  $A(f, r)$ . We assumed that the spectral amplitudes vary slowly with distance and that the undulations of the data are related to site effects. Thus, we looked for monotonic curves with a reasonable degree of smoothness. A more detailed description of this method can be found in Castro *et al.* (1990, 1996, 2003). Figure 6 shows an example of the observed amplitudes and the attenuation functions obtained for one of the events of our data set. The shape of the attenuation func-

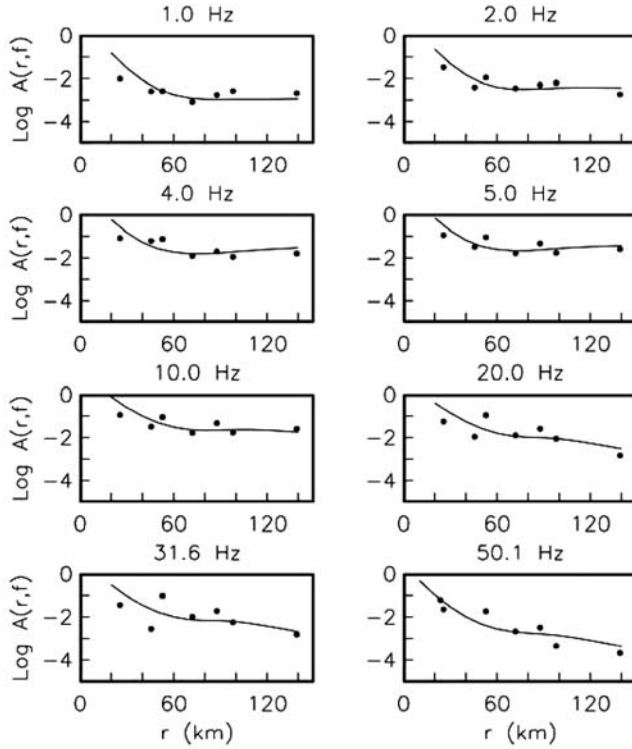


**Figure 6.** Examples of nonparametric attenuation functions obtained for eight different frequencies. The dots are observed  $S$ -wave spectral amplitudes calculated from an  $M$  2.5 earthquake recorded between 25.6 km and 139.0 km.

tions shown is the same for other events except that they may shift upwards or downwards if the size of the source term is larger or smaller, respectively.

Equation (3) can be also expressed as

$$\underline{G} \cdot \underline{m}^{\text{est}} = \underline{d}^{\text{obs}}, \quad (4)$$

where  $\underline{m}^{\text{est}}$  is the vector containing the model parameters (i.e.,  $a_1, \dots, a_j$  and  $s_1, \dots, s_i$ ). Once we determine  $\underline{m}^{\text{est}}$ , we can calculate the predicted data vector

$$\underline{d}^p = \underline{G} \cdot \underline{m}^{\text{est}}. \quad (5)$$

The site response  $z_j$  can be estimated as

$$z_j = \left[ \frac{1}{k} \sum_{i=1}^k (d_i^{\text{obs}} - d_i^p) \right]_j, \quad j = 1, \dots, L, \quad (6)$$

where  $k$  is the number of earthquakes recorded by station  $z_j$ , and  $L$  is the number of sites analyzed.

The attenuation functions can be used to analyze various sources of attenuation and to estimate the quality factor  $Q$  assuming a homogeneous attenuation model of the form

$$A(f, r) = G(r) e^{-\pi f R / v Q} e^{-\pi f K_0}. \quad (7)$$

The first term on the right side of equation (7) accounts for geometrical spreading, the second term for amplitude decrease due to anelasticity, and the third one for near-surface attenuation. The parameter  $v$  is the average wave velocity, 3.4 km/sec for  $S$  waves and 5.8 km/sec for  $P$  waves, based on the crustal structure reported by Harder and Keller (2000) for this region.  $Q$  is the quality factor,  $R = (r - 10)$ ,  $K_0$  the average decay parameter, and  $G(r)$  the geometrical spreading function, which can be approximated as

$$G(r) = \begin{cases} 10/r, & r < r', \\ 10/(r'r)^{1/2}, & r \geq r'. \end{cases} \quad (8)$$

$r'$  is the distance at which the geometrical spreading starts having smaller effect on the amplitude decay due to surface-wave arrivals. We defined  $r' = 80$  km based on the change of rate of amplitude decay observed on the attenuation functions (Fig. 7).

Equations (7) and (8) are normalized at 10 km because we do not have information at closer distances (Fig. 2).

$Q$  and  $K_0$  can be estimated at each frequency by linearizing equation (7) by taking logarithms; thus we can write

$$a(R) = mR + b, \quad (9)$$

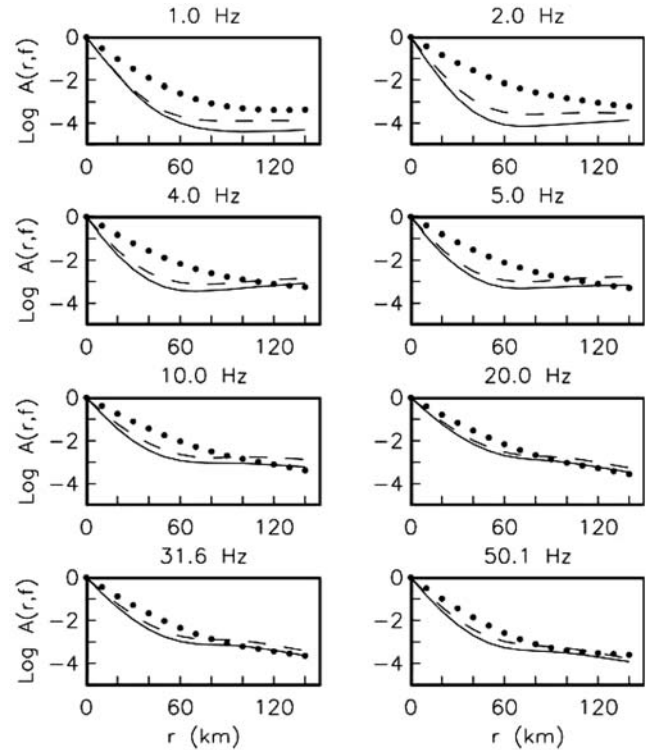


**Figure 7.** Examples of attenuation functions obtained from ground velocity records. The dots correspond to regional  $S$  waves, and the solid and dashed lines to  $P$  and  $S$  waves, respectively, of local earthquakes of the fault zone that ruptured in 1887.

where  $a(R) = \log A(f, r) - \log G(r)$ ,  $m = -\pi f \log e / Qv$ , and  $b = -\pi f \log e K_0$ . The slope  $m$  is estimated by a least-squares fit of equation (9) (e.g., Castro *et al.*, 2003, 2004). For a given frequency  $f$ ,  $Q$  can be estimated, making

$$Q(f) = \frac{\pi f \log e}{mv} \quad (10)$$

and

$$K_0(f) = \frac{b}{\pi f \log e}. \quad (11)$$

## Results and Discussion

We determined attenuation functions for the regional paths (Fig. 4) of  $S$  waves recorded in the velocity channel. For the region near the 1887 earthquake rupture (Fig. 5), we calculated attenuation functions based on acceleration and velocity records of the  $S$  waves and the vertical ground velocity component of the  $P$  waves. Condori (2006) compared attenuation functions obtained with individual components of ground acceleration of the RESNES array and did not observe significant differences between attenuation functions obtained from east–west components and those obtained from north–south components. This suggests that the anisotropy of the crust in northeastern Sonora has a minimum effect on the attenuation estimates. In this article, we combined both horizontal components to calculate the  $S$ -wave attenuation functions in the near-fault zone.

Figure 7 shows regional and near-1887 rupture zone attenuation functions obtained at different frequencies. The spectral amplitudes of the regional functions, obtained from  $S$  waves, decay slower than the near-1887 rupture zone curves obtained from both  $P$  and  $S$  waves. This result indicates greater body wave attenuation near the 1887 rupture. It is interesting to note in this figure that the functions obtained from the  $P$  waves (solid lines) attenuate more than those obtained from  $S$  waves. Figure 8 shows the root mean square (rms) residuals calculated for each distance. On the average, for  $r > 20$  km, the residuals are less or equal to 0.4. At shorter distances, where less data are available, the attenuation functions have rms residuals between 0.8 and 1.6.

We used the attenuation functions obtained at 23 frequencies (0.4–63.1 Hz) to estimate  $Q$  with equation (10). Figure 9 shows the individual estimates of  $1/Q(f) \pm 1$  standard deviation for  $S$  waves obtained from ground velocity records. To describe the observed frequency dependence of the estimated values of  $Q$ , we used the functional form

$$Q(f) = Q_0 f^\eta, \quad (12)$$

where  $Q_0$  is the value of  $Q$  at 1.0 Hz.

Figure 9 also shows the least-squares fit obtained with the estimates of  $Q$  in the 0.4–63-Hz frequency band. For the zone near the 1887 rupture,  $Q_S = 35.9 f^{1.1}$ , whereas for the

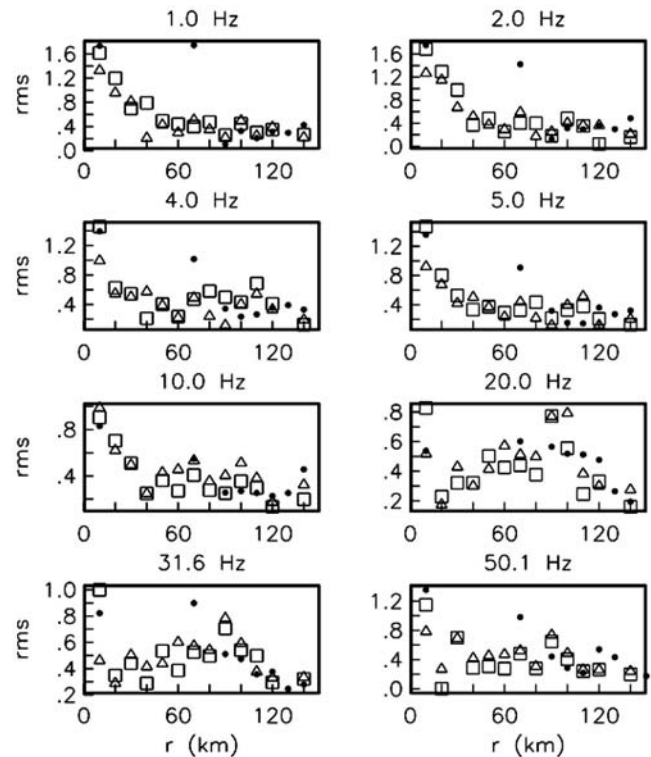


**Figure 8.** The rms residuals calculated for each distance from the nonparametric attenuation functions are shown in Figure 7. Residuals from regional  $S$ -wave attenuation functions, dots; residuals from near-1887 rupture paths of  $S$  and  $P$  waves, squares and triangles, respectively.

regional paths,  $Q_S = 31.6 f^{0.9}$ . This indicates that the attenuation component due to anelasticity is similar in both regions. In contrast, the near-surface attenuation is greater near the 1887 rupture, as can be seen in Figure 10 from the  $K_0$  values obtained by solving equations (9) and (11). At 1 Hz, for instance,  $K_0$  is a factor of 1.9 greater in the region of the 1887 rupture and even greater at higher frequencies. The greater near-surface attenuation in this region is probably due to a combined effect between scattering produced by the highly fractured fault zone and the complex mixture of sedimentary and extrusive rocks of the San Bernardino Valley, where the 1887 rupture zone is located.

To understand the characteristics of the high-frequency attenuation of this rupture zone, we also estimated empirical functions with  $P$  waves recorded on the vertical component of ground velocity (solid lines in Fig. 7) and with  $S$  waves of the horizontal components of the ground acceleration. We then calculated  $Q$  with the same procedure already described previously. Figure 11, which compares our  $P$ - and  $S$ -wave estimates of  $Q$ , indicates greater attenuation for  $P$  waves ( $Q_P = 20.8 f^{1.1}$ ) than for  $S$  waves ( $Q_S = 83.8 f^{0.9}$ ). This can be also seen in Figure 12, where we plotted the  $Q_S/Q_P$  ratio as a function of frequency;  $Q_S/Q_P$  is greater than 1.9 for the whole frequency band shown. This ratio is useful to find the attenuation mechanism of  $Q$ . For instance, Sato (1984) predicted  $Q_S/Q_P = 2.4$  for high-frequency

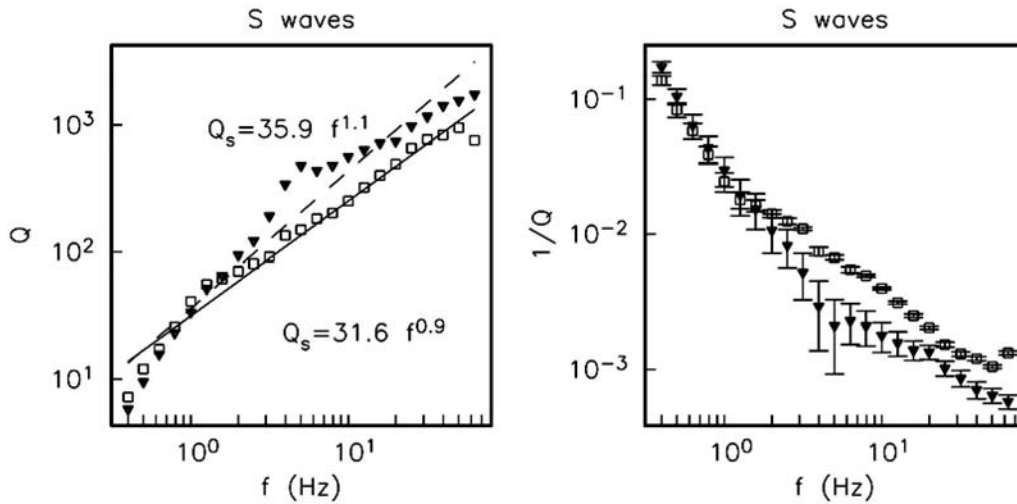


**Figure 9.** Estimates of  $1/Q \pm 1$  standard deviation (right frame) and  $S$ -wave  $Q$  (left frame). The squares correspond to regional paths and the triangles to the zone near the 1887 rupture.

Rayleigh-wave scattering, whereas  $Q_S/Q_P > 1$  was reported for dry rocks from laboratory measurements (Toksoz *et al.*, 1978; Johnston, 1981). On the other hand, for intrinsic shear losses, it is expected that  $Q_S/Q_P = 4/9$  (Anderson *et al.*, 1965), whereas for most types of scattering,  $Q_S/Q_P \geq 1$  (Hough and Anderson, 1988). It thus may be that the ratio of  $Q_S/Q_P > 1.9$  that we obtained for the region near the 1887 rupture zone is mainly caused by scattering.

To verify the consistency between the estimates of  $Q$  and  $K_0$  (Figs. 9, 10, and 11) and the nonparametric attenuation functions (Fig. 7), we calculated the expected spec-

tral amplitudes with equation (7). Figure 13 compares the  $S$ -wave nonparametric attenuation functions (dots) with the expected spectral amplitudes (solid line) as a function of distance for eight different frequencies. We did the same for the  $P$  waves and found, as shown in Figure 13, that in both cases, equation (7) provides spectral amplitudes consistent with the nonparametric functions.

Studies in the Basin and Range province report values of  $Q_{L_g}$  between 138 and 774 (Aleqabi and Wyssession, 2006), but most estimates give values of  $Q$  between 200 and 300 (Singh and Herrmann, 1983; Chavez and Priestley, 1986;

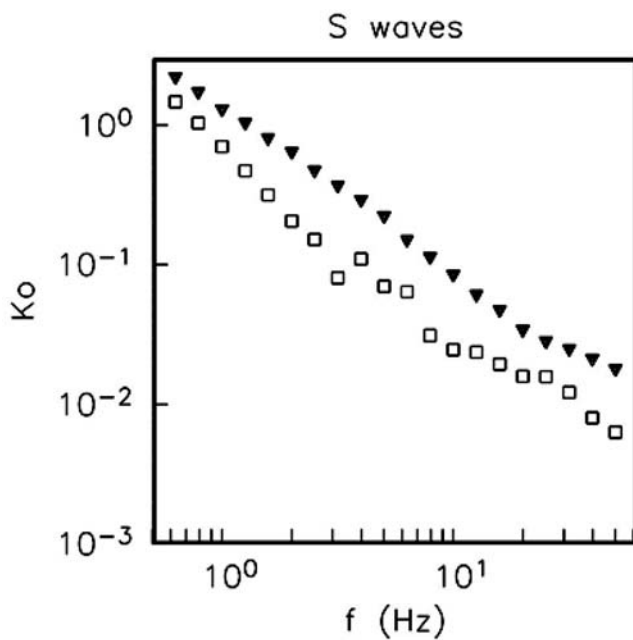


**Figure 10.** Estimates of the near-surface attenuation parameter  $K_0$ . The squares correspond to regional paths and the triangles to the zone near the 1887 rupture.

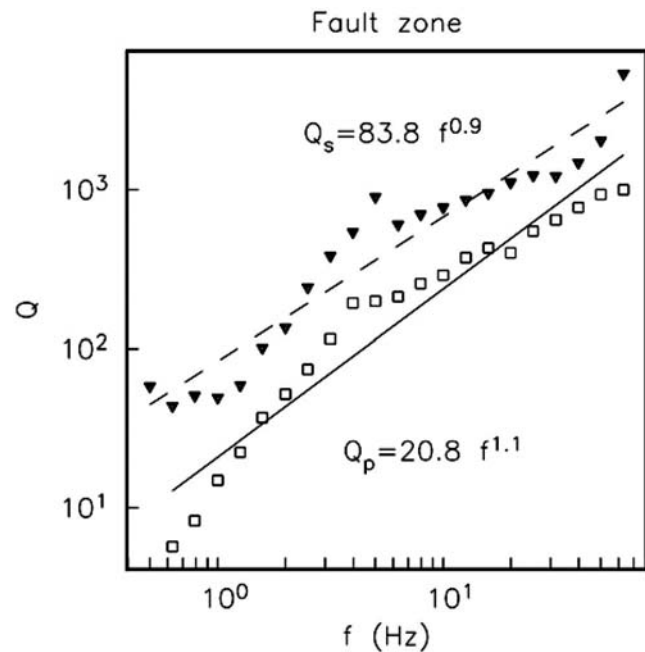


**Figure 11.** Body-wave estimates of  $Q$  for the zone near the faults that ruptured in the 1887 earthquake.  $P$  waves, triangles;  $S$  waves, squares. The lines are least-squares fits of the  $Q$  values.

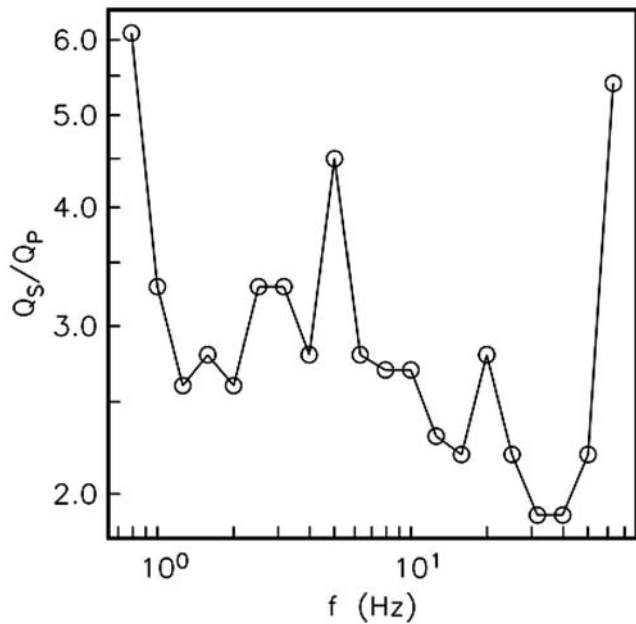


**Figure 12.**  $Q_S/Q_P$  ratios calculated from the  $Q$  values shown in Figure 11.

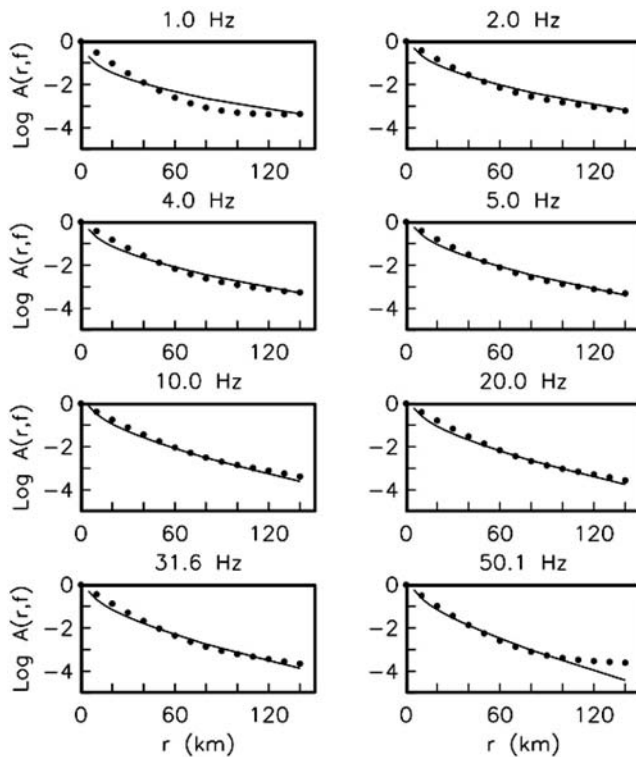


**Figure 13.** Nonparametric attenuation functions (dots) estimated from  $S$ -wave spectral amplitudes of regional source-station paths (curves plotted also with dots in Fig. 7). The solid lines are the expected amplitudes calculated with equation (7) using the  $Q$  and  $K_0$  values shown with squares in Figures 9 and 10, respectively.

Xie and Mitchell, 1990; Benz *et al.*, 1997; Baqer and Mitchell, 1998). These values are consistent with our estimates of  $Q_S$  near 4 Hz ( $Q_S = 83.8f^{0.9}$ ). Estimates of  $Q_0$  based on  $L_g$  coda have been reported for different parts of the world. Cong and Mitchell (1998) found that  $Q_0$  varies between 350 and 450 throughout most of the Arabian peninsula. De Souza and Mitchell (1998) reported for the western margin of the South American continent that  $250 < Q_0 < 450$ . The lapse-time dependence of coda  $Q$  estimates has been studied by different authors; for instance, Gupta *et al.* (1998) found in the Koyna region of India a significant increase of  $Q_0$  with lapse-time-window lengths (from 66 for a lapse-time window of 20 sec to 182 for 60 sec). Thus, it may not be pertinent to compare our estimates of  $Q_0$  with other estimates based on coda waves.

Smith *et al.* (1989) also estimated regional values of  $Q$  in the southern Great Basin of the Basin and Range province and obtained  $Q_S$  values between 255 and 587 in the frequency band of 5–25 Hz. These values are comparable with our  $Q_S$  regional estimates ( $Q_S = 31.6f^{0.9}$ ) in the 10–25 Hz band.

Low  $Q$  values are usually associated with unconsolidated sediments, but have also been reported from fault zones (Malin *et al.*, 1988). Consolidated rocks like granite may also exhibit low  $Q$  values; for instance, Abercrombie (1997) finds  $Q_P \sim 50$  and  $Q_S \sim 23$  in the upper 2.9 km at the granite site in the Cajon Pass borehole.

The low estimated  $Q$  values (Fig. 11), particularly at low frequencies ( $f < 3$  Hz) may be the result of the sedimentary fill of the basins of northeastern Sonora, such as the San Bernardino basin and the complex Basin and Range structure of this region.

## Conclusions

The nonparametric attenuation functions for local and regional earthquakes recorded in northeastern Sonora by the RESNES array indicate that the body waves attenuate more near the 1887 earthquake fault zone compared with the regional  $S$  waves. Although the estimates of  $Q_S$  in the region near the rupture zone are similar to the regional values, the near-surface attenuation is considerably greater than that calculated with the regional data set. At high frequencies (10–25 Hz) the regional values of  $Q_S$  are consistent with estimates reported in the southern Great Basin of Nevada (Smith *et al.*, 1989). In the region of the 1887 rupture, our  $P$ - and  $S$ -wave estimates of  $Q$  indicate greater attenuation for  $P$  waves ( $Q_P = 20.8f^{1.1}$ ) than for  $S$  waves ( $Q_S = 83.8f^{0.9}$ ) in the 0.63–63.1 Hz frequency band. The  $Q_S/Q_P > 1.9$  ratio calculated with local estimates of  $Q$  within the frequency band analyzed (0.63–63.1 Hz) suggests scattering to be an important mechanism controlling the observed decay of the spectral amplitudes with distance.

## Acknowledgments

This research was funded by the Mexican National Council for Science and Technology (CONACYT, Grant Number G33102-T). Luis Inzunza and Antonio Mendoza helped us prepare the maps. Miguel Navarro and Tito Valdez participated in the installation of the seismic stations. We thank Martín Chapman and the anonymous reviewers for their comments and suggestions.

## References

- Abercrombie, R. E. (1997). Near-surface attenuation and site effects from comparison of surface and deep borehole recordings, *Bull. Seismol. Soc. Am.* **87**, 731–744.
- Aguirre-Díaz, G. J., J. Nieto-Obrigón, and F. R. Zúñiga (2005). Seismogenic Basin and Range and intra-arc normal faulting in the central Mexican Volcanic Belt, Querétaro, México, *Geol. J.* **40**, 215–243.
- Aleqabi, G. I., and M. E. Wyssession (2006).  $Q_{L_g}$  distribution in the Basin and Range province of the western United States, *Bull. Seismol. Soc. Am.* **96**, 348–354.
- Anderson, J. G., and Y. Lei (1994). Nonparametric description of peak acceleration as a function of magnitude, distance and site in Guerrero, Mexico, *Bull. Seismol. Soc. Am.* **84**, 1003–1017.
- Anderson, J. G., and R. Quas (1988). The Mexico earthquake of September 19, 1985: effect of magnitude on the character of strong ground motion: an example from the Guerrero, Mexico strong motion network, *Earthq. Spectra* **4**, 635–646.
- Anderson, D. L., A. Ben-Menahem, and C. B. Archambeau (1965). Attenuation of seismic energy in the upper mantle, *J. Geophys. Res.* **70**, 1441–1445.
- Aranda-Gómez, J. J., J. F. Luhr, T. B. Housh, C. B. Connor, T. Becker, and C. D. Henry (2003). Synextensional Pliocene–Pleistocene eruptive activity in the Camargo volcanic field, Chihuahua, México, *Geol. Soc. Am. Bull.* **115**, 298–313.
- Bakun, W. H. (2006). MMI attenuation and historical earthquakes in the Basin and Range province of western North America, *Bull. Seismol. Soc. Am.* **96**, 2206–2220.
- Baqer, S., and B. J. Mitchell (1998). Regional variation of Lg coda  $Q$  in the continental United States and its relation to crustal structure and evolution, *Pure Appl. Geophys.* **153**, 613–638.
- Benz, H. M., A. Frankel, and D. M. Boore (1997). Regional Lg attenuation for the continental United States, *Bull. Seismol. Soc. Am.* **87**, 606–619.
- Brand, D. D. (1937). The natural landscape of northwestern Chihuahua, *University of N.M. Bull. Geol. Ser.* **5**, no. 2, 1–74.
- Brillinger, D. R., and H. K. Preisler (1984). An exploratory analysis of the Joyner–Boore attenuation data, *Bull. Seismol. Soc. Am.* **74**, 1441–1450.
- Castro, R. R., J. G. Anderson, and S. K. Singh (1990). Site response, attenuation and source spectra of S waves along the Guerrero, México, subduction zone, *Bull. Seismol. Soc. Am.* **80**, 1481–1503.
- Castro, R. R., H. Fabriol, M. Bour, and B. Le Brun (2003). Attenuation and site effects in the region of Guadeloupe, Lesser Antilles, *Bull. Seismol. Soc. Am.* **93**, 612–626.
- Castro, R. R., M. R. Gallipoli, and M. Mucciarelli (2004). An attenuation study in southern Italy using local and regional earthquakes recorded by the seismic network of Basilicata, *Ann. Geofis.* **47**, 1597–1608.
- Castro, R. R., F. Pacor, A. Sala, and C. Petrongaro (1996). S wave attenuation and site effects in the region of Friuli, Italy, *J. Geophys. Res.* **101**, 22,355–22,369.
- Castro, R. R., O. M. Romero, and M. Suter (2002). Red sísmica para el monitoreo de la sismicidad del sistema de fallas normales del noreste de Sonora, *Bull. Mex. Geophys. Union* **22**, 379 (in Spanish).
- Chavez, D. E., and K. F. Priestley (1986). Measurement of frequency dependent Lg attenuation in the Great Basin, *Geophys. Res. Lett.* **13**, 551–554.
- Condori, C. (2006). Estudio de atenuación sísmica de la región noreste de Sonora, *Master's Thesis*, División Ciencias de la Tierra, CICESE (in Spanish).
- Cong, L., and B. J. Mitchell (1998). Lg coda  $Q$  and its relation to the geology and tectonics of the Middle East, *Pure Appl. Geophys.* **153**, 563–585.
- De Souza, J. L., and B. J. Mitchell (1998). Lg coda  $Q$  variations across South America and their relation to crustal evolution, *Pure Appl. Geophys.* **153**, 587–612.
- Doser, D. I., and J. Rodríguez (1993). The seismicity of Chihuahua, Mexico, and the 1928 Parral earthquake, *Phys. Earth Planet. Interiors* **78**, 97–104.
- García Acosta, V., and G. Suárez Reynoso (1996). *Los Sismos en la Historia de México*, Universidad Nacional Autónoma de México and Fondo de la Cultura Económica, Mexico City, 718 pp. (in Spanish).
- Gupta, S. C., S. S. Teotia, S. S. Rai, and N. Gautam (1998). Coda  $Q$  estimates in the Koyana region, India, *Pure Appl. Geophys.* **153**, 713–731.
- Harder, S., and G. R. Keller (2000). Crustal structure determined from a new wide-angle seismic profile in southwestern New Mexico, in *New Mexico Geologic Society Guidebook, 51st Field Conference, Southwest Passage: A Trip through the Phanerozoic*, 75–78.
- Henry, C. D., and J. J. Aranda-Gómez (2000). Plate interactions control middle-late Miocene proto-Gulf and Basin and Range, *Tectonophysics* **318**, 1–26.
- Hough, S. E., and J. G. Anderson (1988). High-frequency spectra observed at Anza, California: implications for  $Q$  structure, *Bull. Seismol. Soc. Am.* **78**, 692–707.
- Johnston, D. H. (1981). *Attenuation: A State-of-the-Art Summary, Seismic Wave Attenuation*, SEG Publications, Tulsa, Oklahoma.
- Malagnini, L., R. B. Herrmann, and M. Di Bona (2000). Ground motion scaling in the Apennines (Italy), *Bull. Seismol. Soc. Am.* **90**, 1062–1081.
- Malin, P. E., J. A. Waller, R. D. Borchedt, E. Cranswick, E. G. Jensen, and J. Van Schaack (1988). Vertical seismic profiling of Oroville microearthquakes: velocity spectra and particle motion as a function of depth, *Bull. Seismol. Soc. Am.* **78**, 401–420.
- Ortega, R., and L. Quintanar (2005). A study of the local magnitude scale in the basin of Mexico: mutually consistent estimates of log  $A_0$  and ground-motion scaling, *Bull. Seismol. Soc. Am.* **95**, 605–613.
- Raof, M., R. B. Herrmann, and L. Malagnini (1999). Attenuation and excitation of three component ground motion in southern California, *Bull. Seismol. Soc. Am.* **89**, 888–902.
- Richter, C. F. (1935). An instrumental earthquake magnitude scale, *Bull. Seismol. Soc. Am.* **25**, 1–31.
- Romero, O. M., C. Jacques, and R. R. Castro (2004). Análisis de la sismicidad detectada por la red sísmológica del noreste de Sonora, *Bull. Mex. Geophys. Union* **24**, 230 (in Spanish).
- Sato, H. (1984). Attenuation and envelope formation of three component seismograms of small local earthquakes in randomly inhomogeneous lithosphere, *J. Geophys. Res.* **89**, 1221–1241.
- Singh, S. K., and R. B. Herrmann (1983). Regionalization of crustal coda  $Q$  in the continental United States, *J. Geophys. Res.* **88**, 527–538.
- Smith, K. D., W. R. Walter, R. Castro, K. F. Priestley, and A. R. Anooshepoor (1989). Earthquake clustering near Mina, Nevada, July and August 1987, Nevada Bureau of Mines and Geology Open File Rept. 89-1.
- Spallarossa, D., D. Bindi, P. Augliera, and M. Cattaneo (2002). An  $M_L$  scale in northern Italy, *Bull. Seismol. Soc. Am.* **92**, 2205–2216.
- Stewart, J. H. (1998). Regional characteristics, tilt domains, and extensional history of the late Cenozoic Basin and Range province, western North America (special paper), *Geol. Soc. Am.* **323**, 47–74.
- Suter, M. (1991). State of stress and active deformation in Mexico and western Central America, in *Neotectonics of North America*, D. B. Slemmons, E. R. Engdahl, M. D. Zoback and D. D. Blackwell (Editors), Decade of North American Geology, Vol. 1, Geological Society of America, Boulder, Colorado, 401–421.
- Suter, M. (2001). The historical seismicity of northeastern Sonora and northwestern Chihuahua, Mexico (28–32° N, 106–111° W), *J. South Am. Earth Sci.* **14**, 521–532.

- Suter, M. (2004). A neotectonic–geomorphologic investigation of the prehistoric rock avalanche damming Laguna de Metztlán (Hidalgo State, east-central Mexico), *Rev. Mex. Cienc. Geol.* **21**, 397–411.
- Suter, M. (2006). Contemporary studies of the 3 May 1887  $M_w$  7.5 Sonora, Mexico (Basin and Range province) earthquake, *Seism. Res. Lett.* **77**, no. 2, 134–147.
- Suter, M., and J. Contreras (2002). Active tectonics of northeastern Sonora, Mexico (southern Basin and Range province) and the 3 May 1887  $M_w$  7.4 earthquake, *Bull. Seismol. Soc. Am.* **92**, 581–589.
- Suter, M., M. Carrillo, and O. Quintero (1996). Macroseismic study of shallow earthquakes in the central and eastern parts of the trans-Mexican volcanic belt, Mexico, *Bull. Seismol. Soc. Am.* **86**, 1952–1963.
- Toksoz, M. N., A. H. Johnston, and A. Timur (1978). Attenuation of seismic waves in dry and saturated rocks, I: Laboratory measurements, *Geophysics* **44**, 681–690.
- Trampert, J., H. Paulsen, A. Van Wettum, J. Ritsema, R. Clayton, R. Castro, C. Rebollar, and A. Pérez-Vertti (2003). New array monitors seismic activity near the Gulf of California in México. *EOS* **84**, 29–32.
- Xie, J., and B. J. Mitchell (1990). Attenuation of multiphase surface waves in the Basin and Range province, part I: Lg and Lg coda, *Geophys. J. Int.* **102**, 121–137.
- Yamamoto, J. (1993). Actividad microsísmica en el área de Canatlán, Durango, y su relación con la geología regional, *Geofís. Int.* **32**, 501–510 (in Spanish).
- Zúñiga, F. R., J. F. Pacheco, M. Guzmán-Speziale, G. J. Aguirre-Díaz, V. H. Espíndola, and E. Nava (2003). The Sanfandila earthquake sequence of 1998, Queretaro, Mexico: activation of an undocumented fault in the northern edge of central Trans-Mexican Volcanic Belt, *Tectonophysics* **361**, 229–238.

Centro de Investigación Científica y de Educación Superior de Ensenada (CICESE)  
 División Ciencias de la Tierra Departamento de Sismología  
 Km 107 Carretera Tijuana-Ensenada  
 22860 Ensenada, Baja California, México  
 raul@cicese.mx  
 (R.R.C., C.C.)

Instituto de Geología  
 Universidad Nacional Autónoma de México (UNAM)  
 Estación Regional del Noroeste  
 Apartado Postal 1039  
 83000 Hermosillo, Sonora, México.  
 jacques@geologia.unam.mx  
 (O.R., C.J., M.S.)

Manuscript received 14 March 2007